Applied Physics Letters ARTICLE pubs.aip.org/aip/apl

Field reversal in low pressure, unmagnetized radio frequency capacitively coupled argon plasma discharges

Cite as: Appl. Phys. Lett. **123**, 264102 (2023); doi: 10.1063/5.0179467
Submitted: 2 October 2023 · Accepted: 11 December 2023 ·
Published Online: 27 December 2023

De-Qi Wen,[1,2,a)] Janez Krek,[2] Jon Tomas Gudmundsson,[3,4] Emi Kawamura,[5] Michael A Lieberman,[5] Peng Zhang,[1] and John P Verboncoeur[1,2]

AFFILIATIONS

[1]Department of Electrical and Computer Engineering, Michigan State University, East Lansing, Michigan 48824, USA
[2]Department of Computational Mathematics, Science and Engineering, Michigan State University, East Lansing, Michigan 48824, USA
[3]Science Institute, University of Iceland, Dunhaga 3, IS-107 Reykjavik, Iceland
[4]Division of Space and Plasma Physics, School of Electrical Engineering and Computer Science, KTH Royal Institute of Technology, SE-100 44 Stockholm, Sweden
[5]Department of Electrical Engineering and Computer Sciences–1770, University of California, Berkeley, California 94720, USA

Note: This paper is part of the Special Topic: Plasma Sources for Advanced Semiconductor Applications.
[a)]**Author to whom correspondence should be addressed:** wendeqi@msu.edu

ABSTRACT

In general, the radio frequency (rf) electric field within a sheath points toward the metal electrode in low pressure, unmagnetized rf electropositive capacitively coupled plasma (CCP) glow discharges. This is due to the large ratio of electron to ion mobility and the formation of an ion sheath. In this work, we studied, using fully kinetic particle-in-cell simulations, a reversed electric field induced by the strong secondary electron emission during the phase of sheath collapse in a high-voltage rf-driven low pressure CCP glow discharge. We explored the transition behavior of the formation of field reversal as a function of driving voltage amplitude and found that field reversal starts to form at around 750 V, for a discharge with an electrode spacing of 4 cm at 10 mTorr argon pressure driven at 13.56 MHz. Accordingly, the energy distribution function of electrons incident on the electrode shows peaks from around 3 to 10 eV while varying the driving voltage from 150 to 2000 V, showing potentially beneficial effects in plasma material processing where relatively directional electrons are preferred to solely thermal diffusion electrons.

Radio frequency (rf) capacitively coupled plasma (CCP) sources are essential tools in the high-tech microelectronic industry. CCPs operated at low pressure (a few mTorr) are typically utilized for plasma etching, sputtering, cleaning, and plasma immersed ion implantation due to the more directional ion bombardment on the target through the acceleration across high sheath fields in a less collisional regime.[1–3]

To understand the fundamental plasma physics, rf-driven argon glow discharges, having relatively simple chemistry and few chemical reactions, are commonly studied in the literature.[3–9] The discharges usually have a sheath–plasma–sheath sandwich structure with strong electric fields within the sheath regions adjacent to the powered/grounded electrodes and near-zero electric field within the plasma bulk region. The lighter electrons have higher mobility compared to ions, and respond to the oscillating sheath over time, while the heavy ions respond to the time-averaged sheath electric field, resulting in a nearly static profile and a typical ion sheath. Thus, the electric field within the sheath in general points toward the electrodes from the plasma bulk for electropositive plasma discharges.[1,3]

At high pressures (hundreds of mTorr), a field reversal (the electric field pointing toward the plasma from the surface) in capacitive discharges can be caused by collisions of electrons with the background gas and the corresponding collisional drag force on the electrons. Such collision-driven field reversals have been investigated experimentally, theoretically, and numerically for helium,[10] molecular gases including

hydrogen[10–12] and nitrogen,[13] in single and/or multi-frequency discharges.[14] At a low pressure of 2.3 mTorr, a reversed electric field at the sheath edge during sheath collapse phase was measured experimentally for an argon CCP, and it was attributed to the electron inertial effect.[15] In addition, the presence of a magnetic field tangential to the electrode surface in CCPs was also found to be capable of generating a field reversal during sheath collapse.[16–19] For a floating metal or dielectric surface present in a Hall thruster or negative hydrogen ion source for nuclear fusion applications, the intense emission of electrons[20–22] or negative ions[23] can also cause a reversed electric field along with negative charge excess near the surface, leading to the absence of a conventional Debye or space charge sheath. In principle, in addition to thermal diffusion of electrons, a field reversal can be formed, which then accelerates the electrons toward the electrode to compensate the positive ion current and guarantee a constant (zero) time-averaged current.[11] In CCPs, the field reversal can affect the electron power absorption, ionization dynamics, and the electron and ion energy distributions of the species bombarding the surface.[24] Therefore, it is of importance not only for facilitating the understanding of fundamental physics but also for realistic applications in industry. However, the sheath field reversal induced by secondary electron emission (SEE)[25] from different plasma species and the transition from absence to presence as well as its effect on the plasma characteristic in low pressure CCPs have not been reported.

In this work, we investigate the field reversal due to SEE, its dependence on the driving voltage amplitude, and the energy distribution of electrons incident on electrodes via fully kinetic 1d3v (one-dimensional in space and three-dimensional in velocity) particle-in-cell/Monte Carlo (PIC/MCC) simulations in low pressure rf-driven capacitively coupled argon glow discharges. The surface SEE processes induced by ions, electrons, and excited state atoms, fast ground state neutrals as well as resonant photons are considered. A schematic of the symmetric CCP discharge is shown in Fig. 1.

The PIC/MCC simulation code (oopd1[26–30]) utilized here, incorporating the excited state neutrals including the metastable-level Ar^m, the radiative-level Ar^r, and the 4p-manifold level Ar(4p) as self-consistent space- and time-varying fluids, is strictly benchmarked in a wide pressure range and well validated against experimental measurements[31] at low pressure in our recent works.[32–35] The background gas is assumed to be a spatially uniform fixed fluid at room temperature. The electron-neutral collisions include elastic scattering, excitation to multiple levels of states, and impact ionization. Metastable pooling and stepwise ionization, as well as reactions between excited states are also considered. The corresponding reaction thresholds and cross sections are introduced in our earlier works.[32,33] On the electrode surface, the recombination coefficient for excited states is set to be 0.5 as suggested

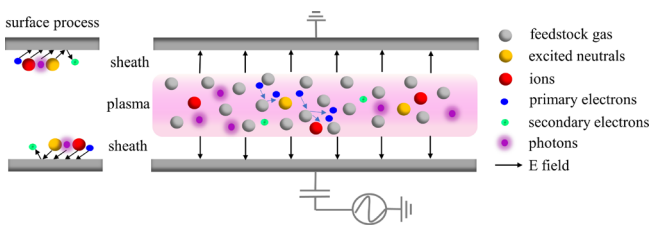

FIG. 1. Schematic of a low pressure, unmagnetized rf capacitively coupled plasma.

by Stewart,[36] i.e., 50% quenched and 50% reflected, and the SEE coefficient is set to 0.21 for Ar^m and Ar^r and 0.27 for Ar(4p).[37] The electron-induced energy- and angle-dependent SEE coefficient is modeled by the empirical Vaughan formula[38] by additionally incorporating a 3% elastic reflection component and 7% inelastic back-scattered component,[35] where the fitting parameters are based on the experimental data by Baglin *et al.*,[39] Furman and Pivi,[40] and Kirby *et al.*[41] The photons from the resonance radiation of Ar^r, with an energy of 11.62 eV, are partially imprisoned at low pressure, and the corresponding SEE coefficient is 0.075 given by the experiments of Feuerbacher and Fitton[42] for a stainless steel electrode. The pressure considered here is 10 mTorr, typically utilized for etching, sputtering, and plasma immersed ion implantation. At this pressure, the ions have few collisions while traveling through the sheath and strike the electrode surface with a high energy, thus, the surface condition of a "clean" electrode[43,44] is adapted for ion-induced SEE. The discharge is driven by a sinusoidal voltage source with driving frequency of 13.56 MHz, and the electrode spacing is fixed at 4 cm. The driving voltage is varied from 150 to 2000 V. In Fig. 2(a), we show the spatiotemporal electric field as a base case with a driving voltage of 1000 V at 10 mTorr. "SEE" in the title represents that all the secondary electron processes are considered in the discharge model. For comparison, Fig. 2(b) shows the spatiotemporal variation of the electric field when the SEE processes are all neglected in the simulation ("No SEE"). Similarly, the spatiotemporal electron power absorption $J \cdot E$ is shown including all the SEE processes in Fig. 2(d) and neglecting all the SEE processes in Fig. 2(e). In addition to the ambipolar diffusion electric field within the region spanned by the sheath motion, an electric field near $x = 0$ cm pointing toward the plasma bulk during the phase of sheath collapse is formed. The thermal electrons are further accelerated to move toward electrode by the positive electric field, resulting in a positive electron power absorption $J \cdot E$ at sheath collapse as shown in Fig. 2(d). With the sheath built up, the secondary electrons accelerated by the sheath field also lead to positive power absorption. Turning off the SEE processes, one can see in Figs. 2(b) and 2(e) that the field reversal and positive electron power absorption vanish, implying that the field reversal is induced by the SEE processes. Decreasing the driving voltage from 1000 to 150 V, but restoring the SEE processes, similarly, field reversal (also positive power absorption at sheath collapse) disappears as shown by comparison of Figs. 2(c) and 2(f). Thus, a transition from negative electric field to positive reversed field during sheath collapse exists while scanning the voltage amplitude, as discussed later.

The formation of the local reversed field facilitates the electron current to balance the ion current over one rf period.[11] However, it is worth noting that a local negative charge excess is present near the electrode surface. Figure 3(a) shows the instantaneous electron density profile for different rf phases $t/T = 0$, 0.25, 0.27, 0.29, and 0.5. The electrons are distinguished into two groups depending on the generation source, i.e., primary electrons (n_e) from electron impact ionization and secondary electrons (n_{se}) from surface emission and/or reflection. The oscillating primary electron density n_e is significantly lower than both the ion density n_i and the secondary electron density n_{se} within the sheath, even at the collapse phase. The secondary electron density n_{se} is higher than n_i near the electrode $x = 0$ cm at sheath collapse $t/T = 0.25$ when the voltage on the powered electrode arrives at its peak. Accordingly, the electric field seen in Fig. 3(b) is positive at $t/T = 0.25$. The emitted secondary electrons have a positive flux and

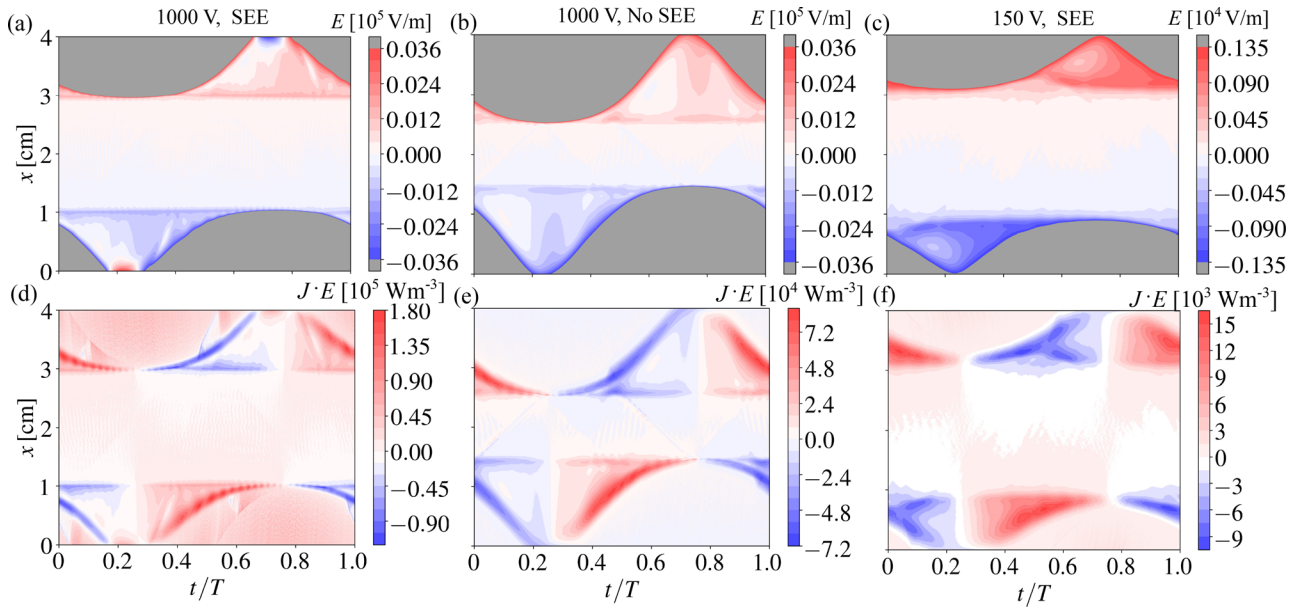

FIG. 2. Spatiotemporal electric field for driving voltage amplitude of (a) 1000 V, in the presence of secondary electron emission (SEE), (b) 1000 V, in the absence of SEE, and (c) 150 V, with SEE; the spatiotemporal deposited electron power density $\langle J \cdot E \rangle$ (d)–(f), respectively. The feedstock gas pressure is 10 mTorr, and the driving frequency is 13.56 MHz, with T the rf period, and the electrode spacing is 4 cm.

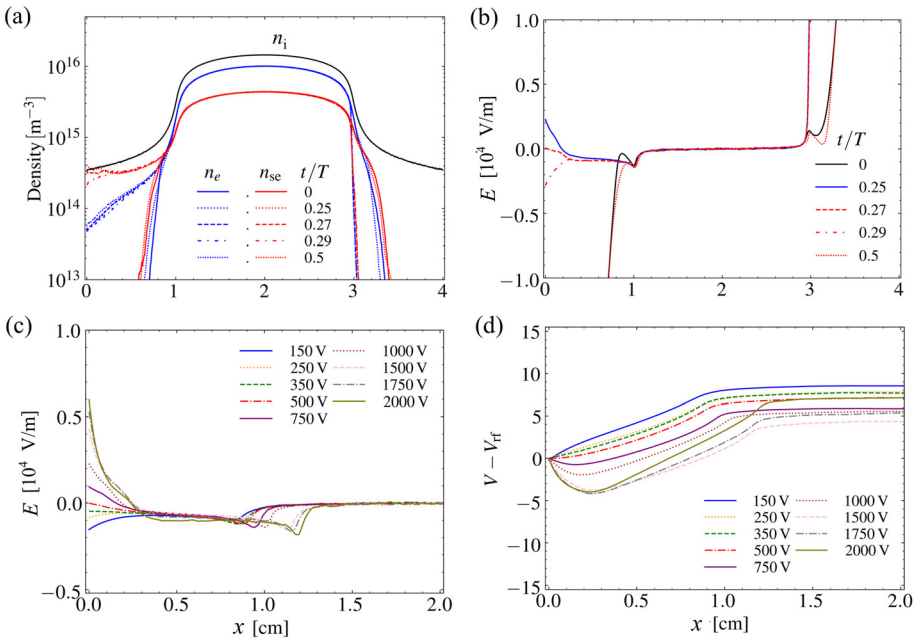

FIG. 3. (a) The plasma density profiles for ions (n_i), primary electrons (n_e), secondary electrons (n_{se}), and (b) electric field at five phases $t/T = 0, 0.25, 0.27, 0.29,$ and 0.5 for a driving voltage amplitude of 1000 V including SEE processes in the discharge model. Panels (c) and (d) show the electric field and voltage profile at the sheath collapse phase $t/T = 0.25$ at various driving voltages from 150 to 2000 V. The gas argon pressure is 10 mTorr, the electrode spacing is 4 cm, and the driving frequency is 13.56 MHz. In panels (c) and (d), the results are shown only for 0–2 cm as the rf discharge is symmetric with respect to the discharge midplane $x = 2$ cm.

tend to move further into the bulk plasma; however, the positive electric field will drag back the secondary electrons. A local minimum potential will be formed and act as a virtual cathode, finally leading to a net negative flux of primary/secondary electrons (not shown here) to balance the ion current during sheath collapse. With increasing rf phase, the local secondary electron density decreases near the surface, and the electric field returns to be negative for $t/T = 0.27$ and 0.29.

Varying the driving voltage from 150 to 2000 V, the spatial electric field and potential drop, $V - V_{rf}$, with V_{rf} being the voltage amplitude at sheath collapse phase $t/T = 0.25$, are plotted in Figs. 3(c) and 3(d), respectively. It is found that the electric field near the electrode surface is around zero for 500 V, and a positive field is formed for 750 V. The reversed field near the electrode is stronger for a higher driving voltage. Note that the electric field near $x = 1.0$ cm is the

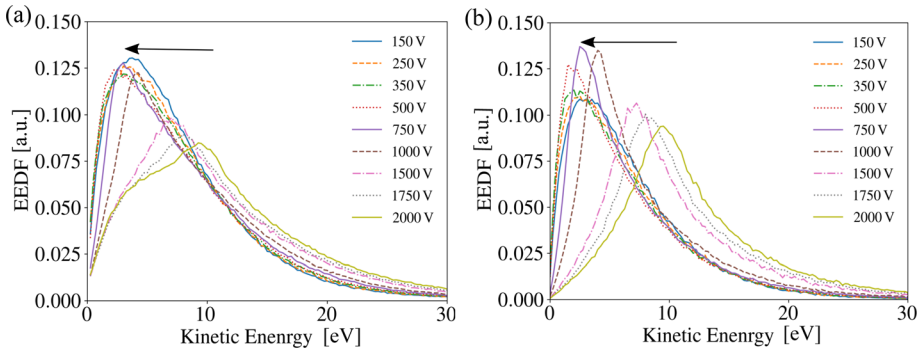

FIG. 4. Time-averaged electron energy distribution function in the energy range of 0–30 eV for (a) all electrons, including primary and secondary electrons, and (b) solely the primary electrons incident on the metal electrode.

ambipolar electric field, which is generated due to the monotonically decaying plasma density from the discharge center toward the electrodes.[45] Accordingly, the spatial potential is always positive when the driving voltage is below 500 V, and a local minimum negative potential starts being formed for voltage above 750 V. The local minimum potential remains almost constant when the voltage is increased further from 1500 to 2000 V. With increasing driving voltage, the plasma ion density increases, along with an increased ion flux flowing toward the electrode. Meanwhile, the ions travel through the sheath almost collisionlessly; thus, the ion impact energy is higher. For a clean electrode condition, the ion-induced SEE coefficient increases slightly for a higher ion impact energy. As a result, more ion-induced secondary electrons could be generated and accelerated by the sheath field to strike the opposite electrode to induce more secondary electron emission again, leading to a stronger reversed field. When the driving voltage is further increased from 1500 to 2000 V, the electron impact energy increases accordingly. Note that the electron-induced SEE coefficient decreases as a function of impact energy when the energy is above 275 eV for stainless steel electrodes (see the SEE coefficient curve in Wen *et al.*[35]). This may be the reason why the field reversal strength is less significantly increased, and the minimum potential is nearly a constant (around −5 V) for driving voltage in the range 1500–2000 V. Figure 4 demonstrates the time-averaged electron energy distribution function (EEDF) in the low energy range for electrons incident on the electrode, and we can see that the reversed electric field increases the peak energy of EEDF up to around 10 eV, much higher than the electron energy of thermal diffusion at low driving voltages.

The formation of a field reversal is highly relevant to the SEE processes, which are determined by the flux of ions Γ_i, excited state neutrals Γ_n, and resonance photons Γ_{ph} flowing toward the surface, of which, the ion flux depends on the plasma ion density. To further analyze the relative importance of different plasma species in generating SEE, Fig. 5(a) displays the peak plasma density at the midplane of the discharge with and without SEE; Figs. 5(b) and 5(c) show the variations of Γ_i, Γ_n, and Γ_{ph} vs driving voltage with and without SEE, respectively. The plasma density is significantly enhanced by the SEE processes in the voltage range of interest from 150 to 2000 V due to electron reflection, scattering and emission along with the ion, and neutral and photon impacts on the electrode surfaces. In the absence of the SEE processes, the plasma density is much lower, and even starts decreasing if the driving voltage is increased further from 1500 to 2000 V. At this scenario, we find that the increased sheath width gradually compresses the plasma bulk region to make it almost disappear at 2500 V (not shown here), and the plasma density further decreases. In Fig. 5(b) with SEE, one can find that the ion flux flowing toward the electrode is larger than the photon and excited state neutral flux. However, note that the SEE coefficient for ions is very close to that of resonant photons, and is around one third of the excited state neutral coefficient in the voltage range of interest. Thus, both the excited state neutrals and resonant photons are important SEE processes that in turn influence the strength of the field reversal. In the absence of SEE processes, the fluxes Γ_i, Γ_n and Γ_{ph} decrease significantly as shown in Fig. 5(c).

In summary, we studied the field reversal during the sheath collapse phase due to the strong SEE induction from ions, electrons,

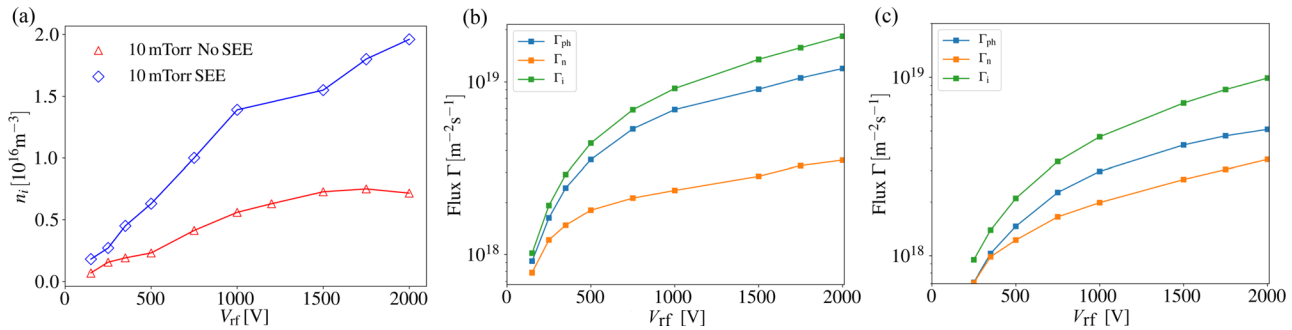

FIG. 5. Time-averaged ion plasma density at the discharge midplane with and without SEE (a), and the flux of plasma species, ions (Γ_i), photons (Γ_{ph}), and excited state neutrals (Γ_n) at each electrode (b) with and (c) without SEE, vs the voltage amplitude in the range 150–2000 V for 10 mTorr gas pressure.

excited state neutrals, and resonant photons bombarding the electrodes in low pressure CCPs. It is found that the formation of field reversal starts for a driving voltage amplitude of around 500 V, while scanning the voltage from 150 to 2000 V. The reversed field is capable of accelerating the electrons to strike the electrode with an energy peak up to 10 eV, much higher than the conventional impact energy from thermal diffusion, showing possible beneficial effects in plasma processing applications where relatively directional electrons can be useful. The excited state neutral and resonant photon fluxes flowing toward the electrode are lower than the ion flux, but of the same order of magnitude. As a result, excited state neutrals and resonance photons are important in affecting the strength of the reversed electric field as their SEE coefficients are almost three times, and close to, the ion SEE coefficient, respectively. In future work, the effects of the pressure and electrode spacing on the field reversal are worth exploring, and a two-dimensional model describing the charge neutralization for structured dielectric surfaces is also worth being developed to explore the importance of directional electrons generated by reversed electric fields with potential applications in plasma processing, such as etching in microelectronics fabrication.

This work was partially supported by the Air Force of Scientific Research (AFOSR) MURI, Grant Nos. FA9550-18-1-0062 and FA9550-21-1-0367, and by the NSF-DOE Partnership, Grant No. DESC0022078, the Icelandic Research Fund, Grant Nos. 163086 and 217999, and a gift from the Applied Materials Corporation, AKT Display Division.

AUTHOR DECLARATIONS

Conflict of Interest

The authors have no conflicts to disclose.

Author Contributions

De-Qi Wen: Conceptualization (equal); Data curation (equal); Formal analysis (equal); Investigation (equal); Methodology (equal); Validation (equal); Visualization (equal); Writing – original draft (lead). **Janez Krek:** Conceptualization (equal); Data curation (equal); Formal analysis (equal); Investigation (equal); Methodology (equal); Validation (equal); Visualization (equal); Writing – review & editing (equal). **Jon Tomas Gudmundsson:** Conceptualization (equal); Formal analysis (equal); Investigation (equal); Methodology (equal); Project administration (equal); Validation (equal); Visualization (equal); Writing – review & editing (equal). **Emi Kawamura:** Conceptualization (equal); Formal analysis (equal); Funding acquisition (equal); Investigation (equal); Methodology (equal); Project administration (equal); Validation (equal); Visualization (equal); Writing – review & editing (equal). **Michael A. Lieberman:** Conceptualization (equal); Formal analysis (equal); Funding acquisition (equal); Investigation (equal); Methodology (equal); Project administration (equal); Validation (equal); Visualization (equal); Writing – review & editing (equal). **Peng Zhang:** Conceptualization (equal); Formal analysis (equal); Funding acquisition (equal); Investigation (equal); Methodology (equal); Project administration (equal); Validation (equal); Visualization (equal); Writing – review & editing (equal). **John P. Verboncoeur:** Conceptualization (equal); Formal analysis (equal); Funding acquisition (equal); Investigation (equal); Methodology (equal); Project administration (equal); Validation (equal); Visualization (equal); Writing – review & editing (equal).

DATA AVAILABILITY

The data that support the findings of this study are available within the article.

REFERENCES

[1]M. A. Lieberman and A. J. Lichtenberg, *Principles of Plasma Discharges and Materials Processing*, 2nd ed. (John Wiley & Sons, New York, 2005).
[2]J. T. Gudmundsson, "Physics and technology of magnetron sputtering discharges," Plasma Sources Sci. Technol. **29**(11), 113001 (2020).
[3]S. Wilczek, J. Schulze, R. P. Brinkmann, Z. Donkó, J. Trieschmann, and T. Mussenbrock, "Electron dynamics in low pressure capacitively coupled radio frequency discharges," J. Appl. Phys. **127**(18), 181101 (2020).
[4]L. Lauro-Taroni, M. M. Turner, and N. S. Braithwaite, "Analysis of the excited argon atoms in the GEC RF reference cell by means of one-dimensional PIC simulations," J. Phys. D: Appl. Phys. **37**(16), 2216–2222 (2004).
[5]L. Wang, P. Hartmann, Z. Donkó, Y.-H. Song, and J. Schulze, "2D particle-in-cell simulations of charged particle dynamics in geometrically asymmetric low pressure capacitive RF plasmas," Plasma Sources Sci. Technol. **30**(8), 085011 (2021).
[6]Z. Donkó, A. Derzsi, M. Vass, B. Horváth, S. Wilczek, B. Hartmann, and P. Hartmann, "eduPIC: An introductory particle based code for radio-frequency plasma simulation," Plasma Sources Sci. Technol. **30**(9), 095017 (2021).
[7]J. P. Verboncoeur, "Particle simulation of plasmas: Review and advances," Plasma Phys. Controlled Fusion **47**(5A), A231–A260 (2005).
[8]L. Wang, P. Hartmann, Z. Donkó, Y.-H. Song, and J. Schulze, "2D particle-in-cell simulations of geometrically asymmetric low-pressure capacitive RF plasmas driven by tailored voltage waveforms," Plasma Sources Sci. Technol. **30**(5), 054001 (2021).
[9]Y.-X. Liu, Q.-Z. Zhang, W. Jiang, L.-J. Hou, X.-Z. Jiang, W.-Q. Lu, and Y.-N. Wang, "Collisionless bounce resonance heating in dual-frequency capacitively coupled plasmas," Phys. Rev. Lett. **107**(5), 055002 (2011).
[10]U. Czarnetzki, D. Luggenhölscher, and H. F. Döbele, "Space and time resolved electric field measurements in helium and hydrogen RF-discharges," Plasma Sources Sci. Technol. **8**(2), 230 (1999).
[11]J. Schulze, Z. Donkó, B. G. Heil, D. Luggenhölscher, T. Mussenbrock, R. P. Brinkmann, and U. Czarnetzki, "Electric field reversals in the sheath region of capacitively coupled radio frequency discharges at different pressures," J. Phys. D: Appl. Phys. **41**(10), 105214 (2008).
[12]D. Vender and R. W. Boswell, "Electron–sheath interaction in capacitive radio-frequency plasmas," J. Vac. Sci. Technol., A **10**(4), 1331–1338 (1992).
[13]M. M. Turner and M. B. Hopkins, "Anomalous sheath heating in a low pressure rf discharge in nitrogen," Phys. Rev. Lett. **69**(24), 3511–3514 (1992).
[14]S. Mohr, E. Schüngel, J. Schulze, and U. Czarnetzki, "Field reversals in electrically asymmetric capacitively coupled radio-frequency discharges in hydrogen," J. Phys. D: Appl. Phys. **46**(43), 435201 (2013).
[15]A. H. Sato and M. A. Lieberman, "Electron-beam probe measurements of electric fields in rf discharges," J. Appl. Phys. **68**(12), 6117–6124 (1990).
[16]L. Wang, D.-Q. Wen, P. Hartmann, Z. Donkó, A. Derzsi, X.-F. Wang, Y.-H. Song, Y.-N. Wang, and J. Schulze, "Electron power absorption dynamics in magnetized capacitively coupled radio frequency oxygen discharges," Plasma Sources Sci. Technol. **29**(10), 105004 (2020).
[17]M. J. Kushner, "Modeling of magnetically enhanced capacitively coupled plasma sources: Ar discharges," J. Appl. Phys. **94**(3), 1436–1447 (2003).
[18]G. Y. Yeom, J. A. Thornton, and M. J. Kushner, "Cylindrical magnetron discharges. II. The formation of dc bias in rf-driven discharge sources," J. Appl. Phys. **65**(10), 3825–3832 (1989).
[19]S. Sharma, I. D. Kaganovich, A. V. Khrabrov, P. Kaw, and A. Sen, "Spatial symmetry breaking in single-frequency CCP discharge with transverse magnetic field," Phys. Plasmas **25**(8), 080704 (2018).
[20]M. D. Campanell, A. V. Khrabrov, and I. D. Kaganovich, "Absence of Debye sheaths due to secondary electron emission," Phys. Rev. Lett. **108**(25), 255001 (2012).

[21]M. D. Campanell, "Negative plasma potential relative to electron-emitting surfaces," Phys. Rev. E **88**(3), 033103 (2013).
[22]D. Sydorenko, I. Kaganovich, Y. Raitses, and A. Smolyakov, "Breakdown of a space charge limited regime of a sheath in a weakly collisional plasma bounded by walls with secondary electron emission," Phys. Rev. Lett. **103**(14), 145004 (2009).
[23]Z. Zhang, B. Wu, S. Yang, Y. Zhang, D. Chen, M. Fan, and W. Jiang, "Formation of stable inverse sheath in ion–ion plasma by strong negative ion emission," Plasma Sources Sci. Technol. **27**(6), 06LT01 (2018).
[24]F. Krüger, S. Wilczek, T. Mussenbrock, and J. Schulze, "Voltage waveform tailoring in radio frequency plasmas for surface charge neutralization inside etch trenches," Plasma Sources Sci. Technol. **28**(7), 075017 (2019).
[25]B. Horváth, M. Daksha, I. Korolov, A. Derzsi, and J. Schulze, "The role of electron induced secondary electron emission from SiO_2 surfaces in capacitively coupled radio frequency plasmas operated at low pressures," Plasma Sources Sci. Technol. **26**(12), 124001 (2017).
[26]J. T. Gudmundsson and M. A. Lieberman, "Ar^+ and Xe^+ velocities near the presheath-sheath boundary in an Ar/Xe discharge," Phys. Rev. Lett. **107**(4), 045002 (2011).
[27]D.-Q. Wen, P. Zhang, J. Krek, Y. Fu, and J. P. Verboncoeur, "Observation of multilayer-structured discharge in plasma ionization breakdown," Appl. Phys. Lett. **119**(26), 264102 (2021).
[28]D.-Q. Wen, P. Zhang, J. Krek, Y. Fu, and J. P. Verboncoeur, "Higher harmonics in multipactor induced plasma ionization breakdown near a dielectric surface," Phys. Rev. Lett. **129**(4), 045001 (2022).
[29]J. T. Gudmundsson, E. Kawamura, and M. A. Lieberman, "A benchmark study of a capacitively coupled oxygen discharge of the oopd1 particle-in-cell Monte Carlo code," Plasma Sources Sci. Technol. **22**(3), 035011 (2013).
[30]A. Proto and J. T. Gudmundsson, "Electron power absorption in radio frequency driven capacitively coupled chlorine discharge," Plasma Sources Sci. Technol. **30**(6), 065009 (2021).
[31]D. A. Schulenberg, I. Korolov, Z. Donkó, A. Derzsi, and J. Schulze, "Multi-diagnostic experimental validation of 1d3v PIC/MCC simulations of low pressure capacitive RF plasmas operated in argon," Plasma Sources Sci. Technol. **30**(10), 105003 (2021).
[32]D.-Q. Wen, J. Krek, J. T. Gudmundsson, E. Kawamura, M. A. Lieberman, and J. P. Verboncoeur, "Benchmarked and upgraded particle-in-cell simulations of capacitive argon discharge at intermediate pressure: The role of metastable atoms," Plasma Sources Sci. Technol. **30**(10), 105009 (2021).
[33]J. T. Gudmundsson, J. Krek, D.-Q. Wen, E. Kawamura, and M. A. Lieberman, "Surface effects in a capacitive argon discharge in the intermediate pressure regime," Plasma Sources Sci. Technol. **30**(12), 125011 (2021).
[34]D.-Q. Wen, J. Krek, J. T. Gudmundsson, E. Kawamura, M. A. Lieberman, and J. P. Verboncoeur, "Particle-in-cell simulations with fluid metastable atoms in capacitive argon discharges: Electron elastic scattering and plasma density profile transition," IEEE Trans. Plasma Sci. **50**(9), 2548–2557 (2022).
[35]D.-Q. Wen, J. Krek, J. T. Gudmundsson, E. Kawamura, M. A. Lieberman, P. Zhang, and J. P. Verboncoeur, "On the importance of excited state species in low pressure capacitively coupled plasma argon discharges," Plasma Sources Sci. Technol. **32**(6), 064001 (2023).
[36]I. M. Stewart, "The reflection of metastable particles at a surface," J. Phys. D: Appl. Phys. **27**(7), 1487–1491 (1994).
[37]S. Schohl, H. A. J. Meijer, M.-W. Ruf, and H. Hotop, "Measurement of yields for electron emission from surfaces upon impact of laser-excited Ar^*(4p) and Kr^* (5p) atoms," Meas. Sci. Technol. **3**(5), 544–551 (1992).
[38]J. R. M. Vaughan, "Secondary emission formulas," IEEE Trans. Electron Devices **40**(4), 830 (1993).
[39]V. Baglin, J. Bojko, O. Gröbner, B. Henrist, N. Hilleret, C. Scheuerlein, and M. Taborelli, "The secondary electron yield of technical materials and its variation with surface treatments," in *Proceedings of the 7th European Particle Accelerator Conference*, 26–30 June 2000, Vienna, Austria, http://www.jacow.org, pp. 217–221.
[40]M. A. Furman and M. T. F. Pivi, "Probabilistic model for the simulation of secondary electron emission," Phys. Rev. Spec. Top.–Accel. Beams **5**(12), 124404 (2002).
[41]R. Kirby and F. King, "Secondary electron emission yields from PEP-II accelerator materials," Nucl. Instrum. Methods Phys. Res., Sect. A **469**(1), 1–12 (2001).
[42]B. Feuerbacher and B. Fitton, "Experimental investigation of photoemission from satellite surface materials," J. Appl. Phys. **43**(4), 1563–1572 (1972).
[43]A. V. Phelps and Z. L. Petrović, "Cold-cathode discharges and breakdown in argon: Surface and gas phase production of secondary electrons," Plasma Sources Sci. Technol. **8**(3), R21–R44 (1999).
[44]A. V. Phelps, L. C. Pitchford, C. Pédoussat, and Z. Donkó, "Use of secondary-electron yields determined from breakdown data in cathode-fall models for Ar," Plasma Sources Sci. Technol. **8**(4), B1–B2 (1999).
[45]J. Schulze, Z. Donkó, A. Derzsi, I. Korolov, and E. Schuengel, "The effect of ambipolar electric fields on the electron heating in capacitive RF plasmas," Plasma Sources Sci. Technol. **24**(1), 015019 (2014).